Effect of HIP at 1000–1200 °C on microstructure and properties of extruded Be-Ti composites

Ramil Gaisin [a],[*], Viacheslav Kuksenko [b], Michael Duerrschnabel [a], Vladimir Chakin [a], Aniceto Goraieb [c], Pavel Vladimirov [a]

[a] Karlsruhe Institute of Technology, Hermann-von-Helmholtz-Platz 1, 76344 Eggenstein-Leopoldshafen, Germany
[b] United Kingdom Atomic Energy Authority, Culham Science Centre, Abingdon, Oxfordshire OX14 3DB, United Kingdom
[c] Karlsruhe Beryllium Handling Facility, Hermann-von-Helmholtz-Platz 1, 76344 Eggenstein-Leopoldshafen, Germany

ARTICLE INFO

ABSTRACT

Solid titanium beryllide blocks will be used for neutron multiplication in the helium-cooled pebble bed (HCPB) blanket concept of EU DEMO. A combination of hot extrusion of Be-Ti powders and subsequent hot isostatic pressing (HIP) of the obtained Be-Ti composites has been proposed for manufacturing such blocks. This work is devoted to the study of the effect of HIP at 1000–1200 °C on the structure and properties of Be-Ti composites in order to optimize the HIP parameters. The HIP at 1000–1200 °C resulted in an almost single-phase titanium beryllide (TiBe$_{12}$) with small amounts of Be and other phases, which gradually dissolve with an increase in the HIP temperature. Such a treatment at 1000 and 1100 °C provides a very fine-grained microstructure of TiBe$_{12}$ with an average grain size of 0.3 and 0.6 μm, respectively. The resulting titanium beryllide is characterized by high microhardness of 1350–1480 HV$_{0.1}$ depending on the HIP temperature. According to the nanoindentation tests of the Be-Ti composite after HIP at 1100 °C, the indentation modulus of TiBe$_{12}$ can be estimated as 295 GPa. The fracture toughness of the TiBe$_{12}$ was determined as 1.5–1.7 MPa·m$^{1/2}$. The temperature of 1100 °C was chosen as optimal for the HIP of Be-Ti composites after hot extrusion. The titanium beryllide obtained in this way was used to manufacture a reduced size mockup of Ø20 mm × 18 mm. The mockup has no visible surface defects and can be used for further experiments.

1. Introduction

Intermetallic titanium beryllide TiBe$_{12}$ is considered as the main neutron multiplier material in the helium-cooled pebble bed (HCPB) blanket concept of the EU DEMO [1]. Titanium beryllide will be used in the form of solid hexagonal blocks with a central hole or blocks of more complex shape [2,3], while the Japanese DEMO concept proposes the use of vanadium beryllide as millimeter-sized pebbles [4–6], although solid blocks are also considered presently. The main advantages of titanium beryllide over the pure beryllium, which it substitutes, are higher operating temperatures, higher corrosion resistance, lower swelling and retention of tritium under neutron irradiation [7–10]. Recently, a series of full size titanium beryllide blocks have been manufactured industrially using vacuum hot pressing [2,3]. One of the alternatives to this technology can be spark plasma sintering of beryllides, which is being actively studied in Japan [11,12]. Another alternative to vacuum hot pressing is hot extrusion of Be-Ti powders and subsequent hot isostatic pressing (HIP) of the extruded Be-Ti rods [13]. However,

the effect of the HIP on the microstructure and the properties of the titanium beryllide obtained has not been systematically studied up to now, and the optimal parameters of the HIP have not been determined. This publication is a logical continuation of the previous work [14], which considered the effect of HIP at 800 and 900 °C on the microstructure and properties of extruded Be-Ti composites. The current work expands knowledge about the effect of higher HIP temperatures and is of practical interest for manufacture of beryllide blocks for the HCPB blanket concept. An additional merit of the current paper is an attempt to manufacture a mockup of such titanium beryllide block by extrusion of Be-Ti and HIP using the selected optimal parameters. The results obtained determine the conditions for the production of beryllide blocks for EU DEMO using the technology under consideration.

2. Materials and experimental techniques

Be-Ti composite rods obtained by hot extrusion of pure Be and Ti powders were taken as the sample material for the study. The ratio of

---

* Corresponding author.

pure beryllium and titanium in the composite is Be-7.7 at.% Ti or Be-30.8 wt% Ti, which corresponds to the target composition of TiBe$_{12}$ beryllide. Further details on the chemical composition of the composite as well as on extrusion can be found in [13–16]. The sections of Be-Ti rods having Ø40 mm × 12 mm were sealed into Nb capsules and subjected to HIP at 1000, 1100, and 1200 °C under argon pressure of 102 MPa for 4 h at the Karlsruhe Beryllium Handling Facility (KBHF). The capsules were heated and cooled at a rate of about 10–20 K/min.

After HIP, the Be-Ti samples were removed from the capsules and cut using a diamond saw or electrical discharge machining. The surfaces of the samples were polished mechanically and/or electrolytically. The samples were examined using scanning electron microscopy (SEM) on a Zeiss Merlin microscope. All SEM micrographs were taken in the secondary electron (SE) mode, with the exception of Fig. 12b, taken in backscattered electrons (BSE). The elemental analysis of the samples was carried out with energy-dispersive X-ray spectroscopy (EDS). Electron backscatter diffraction (EBSD) was used to build surface normal-projected inverse pole figure (IPF-Z) orientation maps. The black and white lines on the maps indicate high- and low-angle grain boundaries, respectively, while silver lines correspond to twin boundaries (in Be-Ti after HIP at 1200 °C). The volume fractions of the phases were determined by the systematic point count method on mechanically polished samples. X-ray diffraction (XRD) measurements were performed on a Seifert PAD II diffractometer with Cu-K$\alpha_{1/2}$ radiation. Microhardness was measured on a Zwick Roell Indentec ZHμ tester using indentation forces of 100–1000 gf. Density was measured by the hydrostatic weighing in C$_{14}$H$_{30}$ liquid medium (Mettler Toledo MS303TS). The density of pure TiBe$_{12}$ of 2.288 g/cm^3 was used to calculate the percentage of theoretical density (TD) of the samples after HIP [17]. Electron-transparent lamellae were prepared by focused ion beam (FIB) on a FEI Scios system and were examined using a Talos F200X transmission electron microscope equipped with a Super X-EDS system for energy-dispersive X-ray spectroscopy, a Gatan Enfinium electron energy-loss spectrometer (EELS), and a scanning unit (STEM) with high-angle annular dark-field (HAADF) detector.

Indentations were conducted using a Keysight G200 nanoindentation system with a diamond pyramid Berkovich tip using the continuous stiffness measurement (CSM) technique [18] with a 42 Hz and 2 nm oscillation. The frame stiffness of the instrument and indenter tip was calibrated using a fused silica sample. To quantify the nanoindentation hardness *H* and indentation modulus *E*, the method proposed by Oliver and Pharr [18] is used, which forms the basis of the indentation testing standard [19]. The following equations were used:

$$H = \frac{P}{A} \tag{1}$$

$$E = \frac{1 - \nu^2}{\frac{1}{E^{eff}} - \frac{1-\nu_i^2}{E_i}} \tag{2}$$

$$E^{eff} = \frac{S\sqrt{\pi}}{2\beta\sqrt{A}} \tag{3}$$

where *A* is the projected contact area of the indentation at load *P*, *ν* is Poisson's ratio of the test piece, 0.09 for TiBe$_{12}$ [20], ν_i is Poisson's ratio of the indenter, 0.07 for diamond , E^{eff} is the effective modulus of the contact between the indenter and the sample, E_i is the modulus of the indenter, 1140 GPa for diamond [19], *S* is the contact stiffness, which is computed as the slope of the unloading curve continuously evaluated in the CSM mode, and *β* is the tip geometry correction factor (1.034 for a Berkovich tip) [21].

During this study, 150 indents were made into the TiBe$_{12}$ in Be-Ti samples after HIP at 1100 °C with a target maximum indentation depth of 1600 nm. Surface position corrections were made for each indentation before data analysis. For consistency, load and contact stiffness data averaged between 1300 and 1500 nm indentation depth

were used to calculate indentation hardness and elastic modulus, avoiding the depth range within which there is a strong indentation size effect.

To assess the fracture properties of TiBe$_{12}$ in Be-Ti samples after HIP at 1100 °C as well as prior particle boundaries, microcantilever fracture tests were carried out [22]. The pentagonal cantilevers were manufactured using FIB milling, following the procedure described in [22] leading to the geometry displayed in Fig. 1.

Each cantilever was tilted at 0° and 45° for dimensional measurements. Typical dimensions of cantilevers used in this study were ≈20 μm in length, ≈4.5 μm in width, and ≈5 μm in height. The fracture testing was performed using a Berkovich tip in an Keysight G200 nanoindenter equipped with a nano-positioning stage. The deflection test was carried out at a displacement rate of 5 nm/s until a sharp load drop occurred and the data was recorded to a maximum preset displacement of 2.5 μm.

3. Results and discussion

3.1. Microstructure

Fig. 2 presents the diffraction patterns of Be-Ti after extrusion and HIP at 1000, 1100, and 1200 °C. All samples are characterized by an almost single-phase structure of TiBe$_{12}$. However, in the case of HIP at 1000 and 1100 °C, a small peak corresponding to the beryllium phase is observed (Fig. 2a,b). Other beryllide phases are not present in the pattern, unlike samples investigated after HIP at 800 and 900 °C [14]. SEM micrographs (Fig. 3) show almost single-phase TiBe$_{12}$ with prior particle boundaries typical for powder materials in the form of a chain of white beryllium oxide particles. These boundaries are elongated along the extrusion direction. In addition to the target titanium beryllide, dark regions are observed corresponding to the residual beryllium phase together with pores, which was discussed in more detail earlier [13,14]. The volume fraction of the beryllium phase together with the pores gradually decreases from 10% to 5%, and the total density increases from 98.4 to 99% with an increase in the HIP temperature from 1000 to 1200 °C (Table 1). The micrographs of Be-Ti after HIP at 1000 °C show bright fuzzy areas usually observed in the centers of former powders (Fig. 3a,b). They can correspond to the Ti$_2$Be$_{17}$ phase, which was observed in the same places in the Be-Ti samples after HIP at 900 °C [14].

Fig. 4 shows EBSD maps built along the extrusion direction after HIP at 1000–1200 °C. All samples are characterized by a homogeneous grain structure with no visible microtexture. Black areas in the maps correspond to non-indexed beryllium oxide particles at the prior particle boundaries. Be-Ti after HIP at 1000 °C has a very fine-grained structure of 0.1–0.6 μm with an average grain size of 0.28 μm. The grain size in Be-Ti after HIP at 1100 °C is also quite small and was determined to be in the range of 0.2–1.3 μm with an average size of 0.64 μm. In more detail, the microstructure after HIP at 1100 °C, including TEM study, was discussed earlier [13]. In contrast, HIP at 1200 °C leads to significant grain growth. The range of grain sizes is 1–7 μm, and the average grain size is 3.4 μm. In addition, after HIP at 1200 °C, some grains have 60° twins (highlighted in silver in Fig. 4c). The presence of such defects may indicate the accommodative deformation via twinning of large grains at 1200 °C. A similar twinning in NbBe$_{12}$ was observed in [23,24].

Fig. 5 presents the results of EDS for a Be-Ti sample after HIP at 1000 °C. Elemental maps show a slightly higher titanium content along the central axis of the former powder particles. At the prior particle boundaries, an increased oxygen content is observed, which is associated with beryllium oxide particles. The composition of such oxides has been confirmed by TEM studies earlier [13]. Areas with an increased titanium content, which can also be seen in Fig. 3a, b, indicate that HIP at 1000 °C was insufficient for the complete dissolution of the residual intermediate beryllide phases (presumably Ti$_2$Be$_{17}$). In the previous work [13], such an increase in the amount of titanium after HIP at 1100 °C was not observed, however, single undissolved particles with an
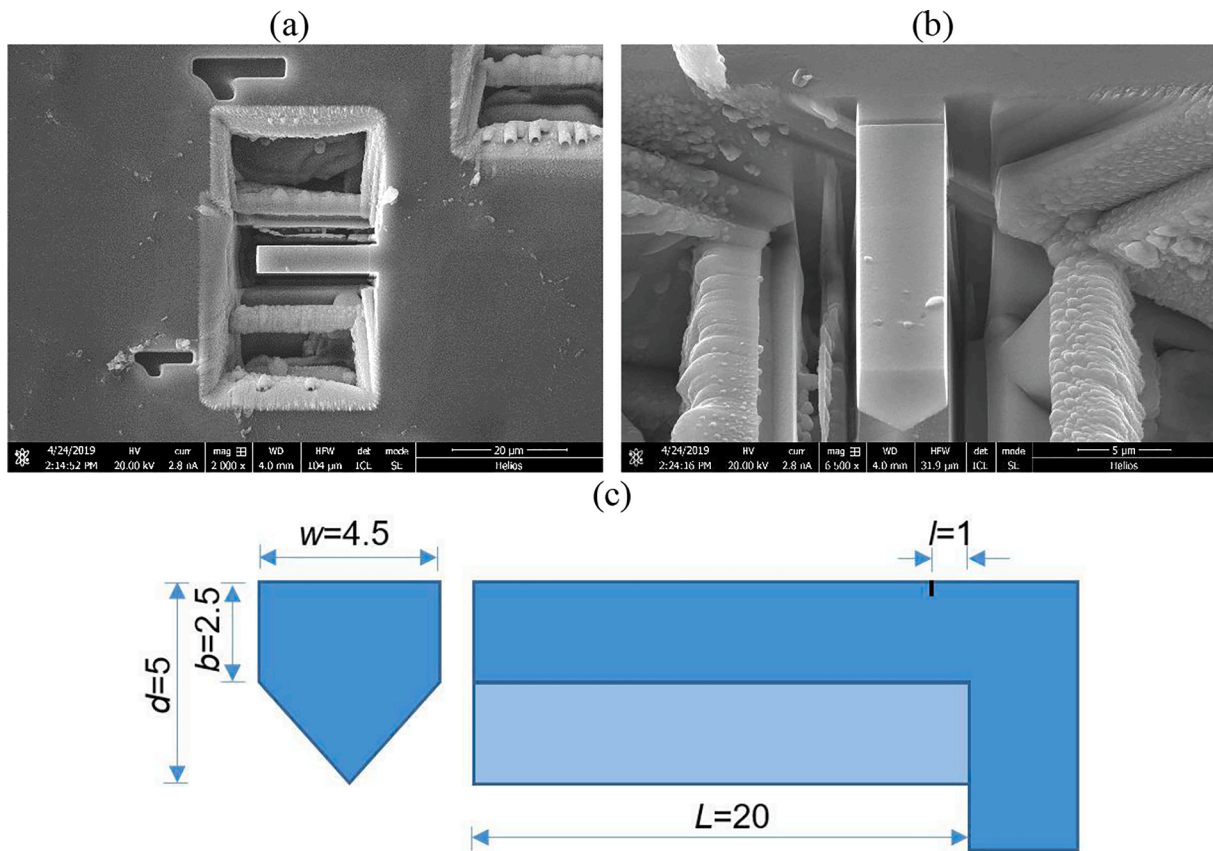
Fig. 1. (a,b) General geometry of the cantilevers prepared with FIB in the $TiBe_{12}$ sample and (c) their typical dimensions in μm. Two types of cantilevers have been tested: i) straight-notched cantilevers for fracture in the $TiBe_{12}$ grains; ii) straight-notched cantilevers for fracture at the prior particle boundaries.
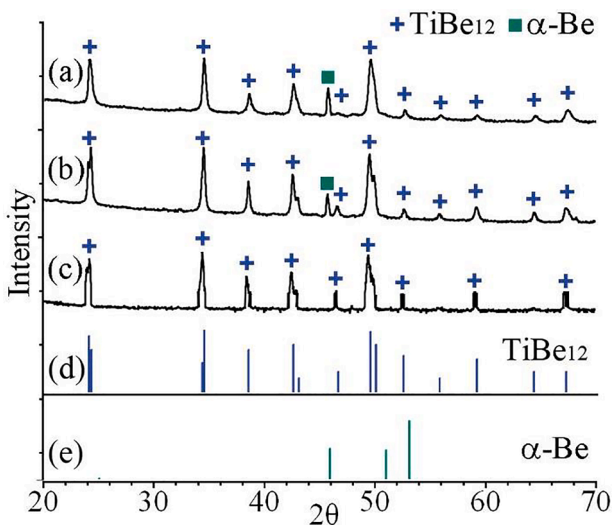

Fig. 2. (a-c) X-ray diffraction patterns of Be-Ti composites after extrusion and HIP at (a) 1000 °C, (b) 1100 °C, and (c) 1200 °C. Below the diffraction patterns are the peaks for (d) $TiBe_{12}$ and (e) α-Be used for the analysis.

increased titanium content were found. After HIP at 1200 °C (Fig. 6a), such single particles with a size of up to 20 μm in length are also observed. Fig. 6b-e shows that in addition to the increased titanium content, the particle also has a higher oxygen content inside, as well as increased aluminum and silicon content at the edge of particle. It should be noted that particles with an increased silicon content were found earlier in the study of the transformation of the pure titanium phase into

$TiBe_{12}$ during HIP at 900 °C [14].

For a more detailed study of the microstructure of the particle shown in Fig. 6, lamellae were lifted out using FIB. Fig. 7 shows an overview of a lamella with phases identified by diffraction patterns and EELS. Some beryllide grains could not be identified due to the similarity of the tetragonal $TiBe_{12}$ and rhombohedral Ti_2Be_{17} lattices at particular zone axes (orange areas in Fig. 7b). Their reflections overlap and both structures can be used to describe the experimental pattern. The TEM results clearly show the presence of intermediate beryllides ($TiBe_2$ and Ti_2Be_{17}) in the structure even after HIP at 1200 °C. These data supplement the previously obtained information on the sequential phase transformation during HIP at 900 °C. These data supplement the previously obtained information on the sequential phase transformation at HIP at 900° C.

Further dissolution of intermediate beryllides with an increased titanium content occurs during HIP at 1200 °C and no pure titanium phase can be found. $TiBe_2$ beryllide transforms into Ti_2Be_{17}, and then $TiBe_{12}$, with impurity elements forming a separate extended phase (highlighted in red in Fig. 7). Detailed EDS of this phase (Fig. 8) shows an increased content of Ti, O (not shown, but the distribution is similar to Ti), Al, Si (similar to the distribution of Al), Fe. Apparently, the solubility of these elements in $TiBe_{12}$ and Ti_2Be_{17} is lower than in $TiBe_2$, and higher beryllides (with higher Be content) can grow further upon diffusion of impurities into a separate phase along grain boundaries. A separate study will be devoted to the structure of this new phase. In addition, the HAADF image (Fig. 8a) revealed lines crossing the beryllide phase in the direction of the phase with a high content of impurities. EDS showed that these lines are connected to particles with a higher content of arsenic (Fig. 8f) and phosphorus (not shown, the distribution is similar to As). The content of As and P is usually negligible in beryllium alloys, and such particles deserve a separate further study.
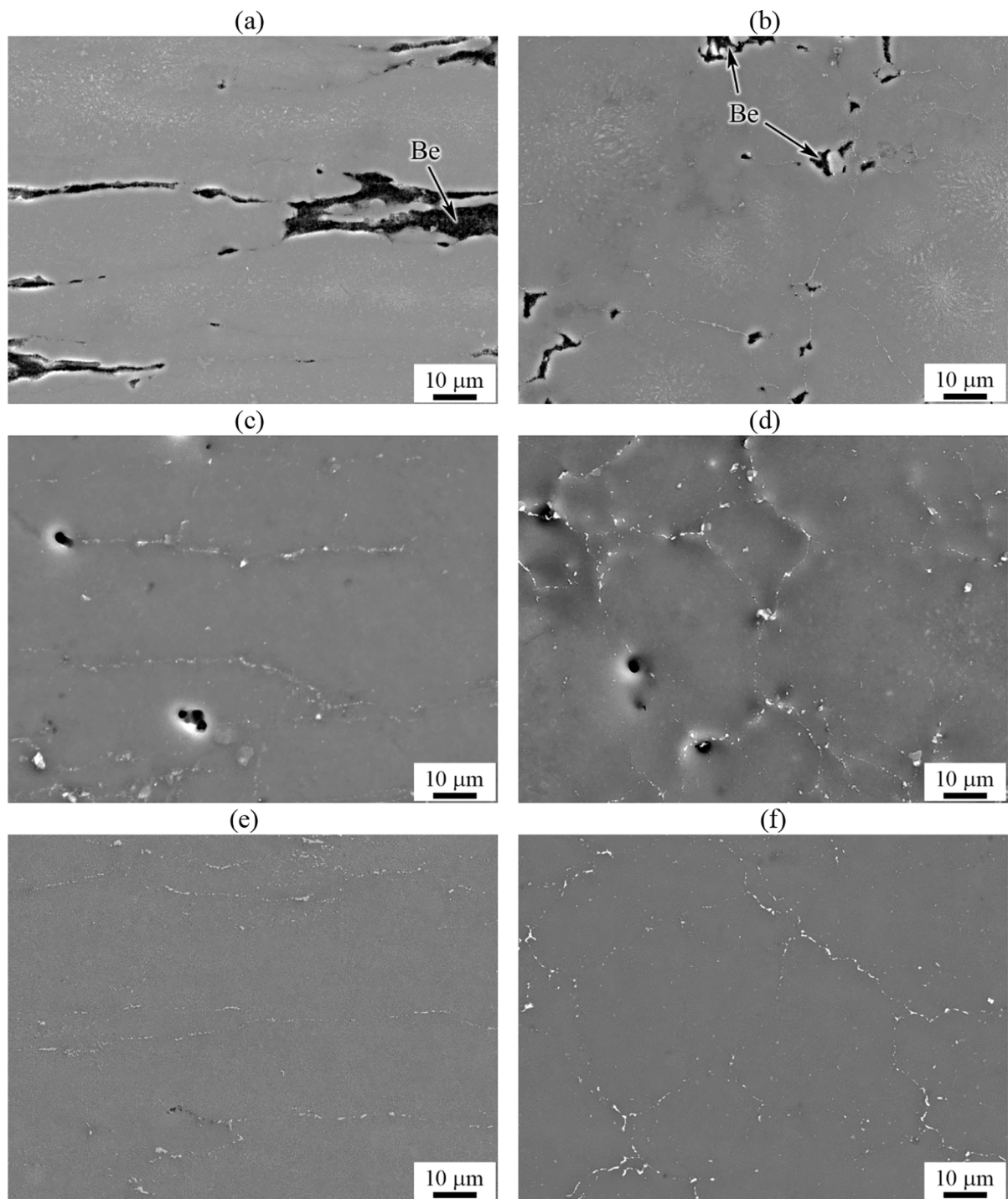
Fig. 3. Microstructure of Be-Ti composites after extrusion and hot isostatic pressing at: (a,b) 1000 °C (c,d) 1100 °C, (e,f) 1200 °C; (a,c,e) along and (b,d,f) across extrusion direction. In (a,c,e), the extrusion direction is horizontal.

The results obtained complete the study of the effect of HIP on the structure and some properties of Be-Ti composites in the temperature range 800–1200 °C. With an increase in the HIP temperature, the reaction of $TiBe_{12}$ beryllide synthesis from beryllium and titanium phases is accomplished to a greater extent, and the volume fractions of beryllium phase and intermediate beryllide phases gradually decrease. Nevertheless, even after HIP at 1100 and 1200 °C, single particles with an increased content of titanium and other impurities are still observed. As previously shown, such particles can cause cracking, probably due to differences in thermal expansion coefficients [13]. In addition, an increase in the HIP temperature 1100–1200 °C leads to a significant increase in the grain size. It was reported, that after HIP at 1100 °C, in addition to relatively large particles of BeO at the prior particle boundaries, a number of BeO nanoparticles are present in the structure at $TiBe_{12}$ grain boundaries [13]. We have suggested that these particles can pin the boundaries and restrict the grain growth leading to smaller grain size even at processing temperatures as high as 1000–1100 °C. Larger grain size may indicate that at 1200 °C the oxide particles inhibit grain growth to a lesser extent, and their size reaches 7 μm. In terms of the use of titanium beryllide in a breeder blanket of fusion reactors, a smaller grain size is more advantageous for more efficient removal of gases formed during irradiation of beryllium, since in this case the

Table 1
Density, phase composition, volume fraction and microhardness of Be-Ti composites depending on the HIP temperature after extrusion.

HIP temperature, °C	Density, g/cm^3	Phase	Volume fraction, %	Microhardness, HV 0.1
1000 °C	2.251	TiBe$_{12}$ + Ti$_2$Be$_{17}$	90	1480 ± 50
		Be + porosity	10	360 ± 30
1100 °C	2.258	TiBe$_{12}$	93	1420 ± 40
		Be + porosity	7	360 ± 30
1200 °C	2.264	TiBe$_{12}$	95	1350 ± 40
		Be + porosity	5	–

diffusion path to the grain boundaries is reduced [25]. But even from this point of view, the grain size obtained after HIP at 1200 °C is acceptable until the grain size reaches hundreds and thousands of microns. Therefore, for the manufacture of a mockup from extruded Be-Ti bars, HIP temperatures of 1100 and 1200 °C were selected.

3.2. Microhardness and nanoindentation

With an increase in the HIP temperature from 1000 to 1200 °C, the microhardness of the beryllide phase slightly decreases from 1480 to 1350 HV$_{0.1}$ (Table 1). At the same time, the hardness of the beryllium phase remains about 360 HV after HIP at 1000 and 1100 °C. After HIP at 1200 °C, the microhardness of the beryllium phase could not be

measured because of its small volume fraction. Compared to the hardness after HIP at 900 °C (1680 HV$_{0.1}$ [14]), the hardness of the beryllide phase in this work is lower, apparently due to the dissolution of other beryllide phases and an increase in the grain size. Further experiments on nanoindentation and fracture tests were carried out for the sample after extrusion and HIP at 1100 °C.

A significant scatter in the values of nanoindentation hardness and modulus was observed in the TiBe$_{12}$. The data exhibit a wide distribution with hardness values ranging from 13.7 to 16.8 GPa and an indentation modulus ranging between 272 and 337 GPa. The average values are 14.9 ± 0.5 GPa and 294.9 ± 8.9 GPa for the hardness and the indentation modulus, respectively. The frequency distribution of the nanoindentation data is shown in Fig. 9. Although data on the crystallographic anisotropy of elastic and plastic properties of TiBe$_{12}$ are unknown, this may be the reason for the observed large scatter of results as well as the difference in grain size, possible residues of intermediate beryllides and other phases.

Comparison of the hardness data for microhardness (1420 HV$_{0.1}$ or 13.93 GPa) and nanoindentation (14.9 GPa) shows that they are close, but as usual, higher hardness corresponds to lower indentation forces. A further increase in the indentation forces to 1 kg led to a microhardness value on average of 1280 HV$_1$ or 12.5 GPa. Obviously, with an increase in the force, more defects, such as grain boundaries, porosity, particles, are deformed together with TiBe$_{12}$, which somewhat decreases the measured hardness values. The evaluated elastic modulus is in good agreement with the values of $E = 280$–282 GPa in [26–28]. Beryllides of other metals have close values of the elastic modulus, for example, NbBe$_{12}$ – 324 GPa [29], ZrBe$_{12}$ – 289 GPa [27], VBe$_{12}$ – 300 GPa [30].
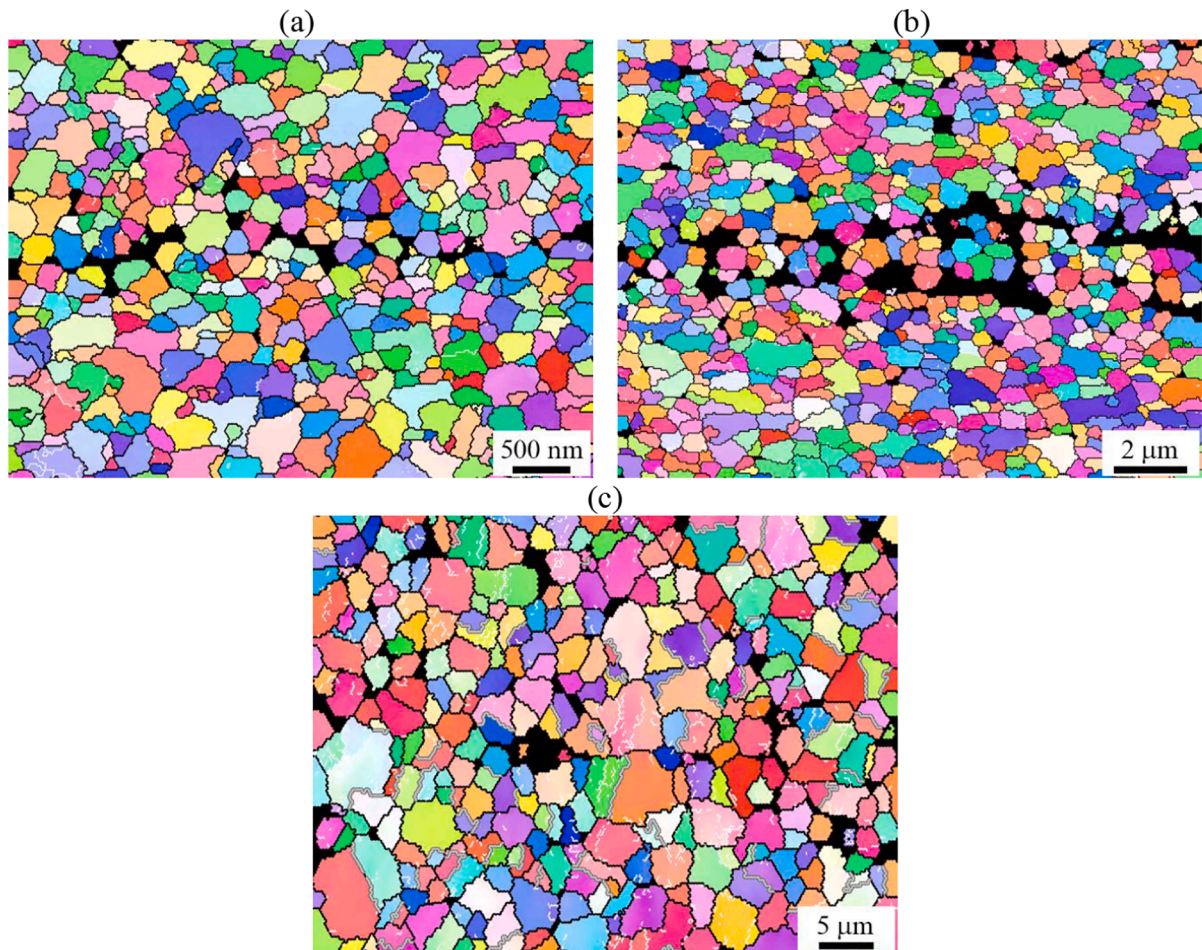

Fig. 4. EBSD maps of TiBe$_{12}$ phase in Be-Ti composites after extrusion and hot isostatic pressing at: (a) 1000°, (b) 1100 °C, and (c) 1200 °C. The black areas in the EBSD maps correspond to non-indexed oxide particles at the prior particle boundaries.
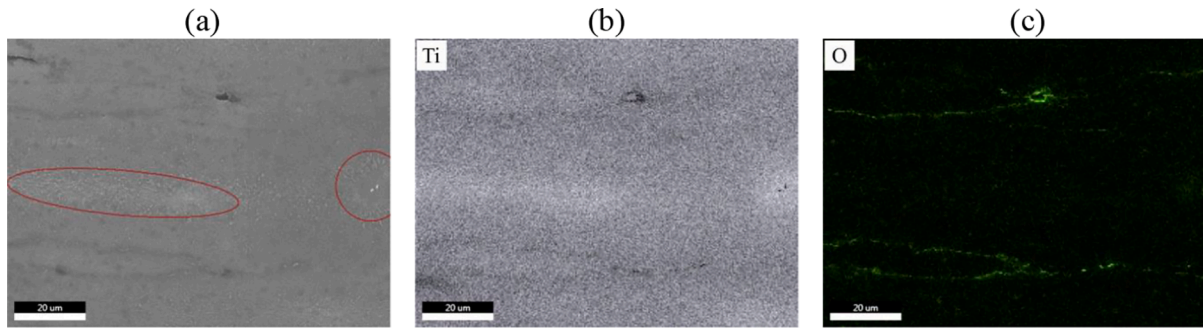
Fig. 5. (a) Microstructure and (b,c) corresponding elemental EDS maps of a Be-Ti composite after extrusion and hot isostatic pressing at 1000 °C: (b) titanium, (c) oxygen. (a) Areas with a higher titanium content are outlined in red. (For interpretation of the references to colour in this figure legend, the reader is referred to the web version of this article.)
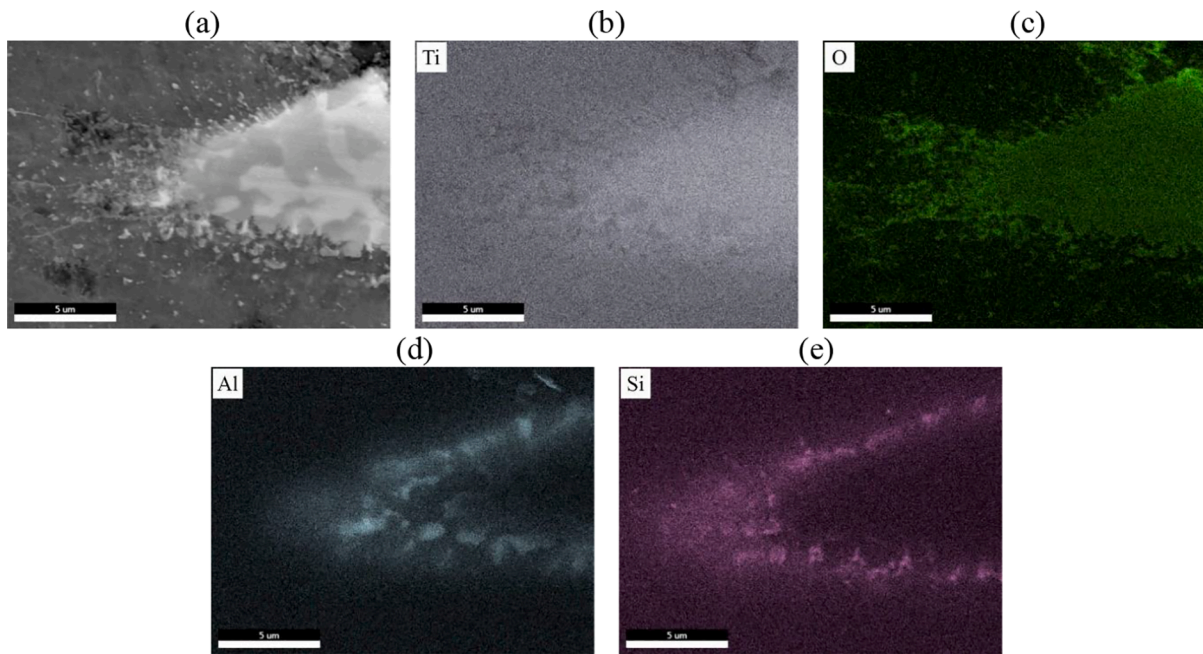

Fig. 6. (a) Microstructure and (b-e) corresponding elemental EDS maps of an undissolved particle in Be-Ti after extrusion and hot isostatic pressing at 1200 °C: (b) titanium, (c) oxygen, (d) aluminum, (e) silicon.

3.3. Microcantilever fracture tests

The results in Fig. 10 show a typical load–displacement plot: load changes linearly until a sudden failure in the load range between 45 and 100 mN, after which the indenter rapidly approaches its displacement limit (2500 nm).

Fracture toughness values K_C were calculated using linear elastic fracture mechanics (LEFM), as in the micromechanical fracture work of Di Maio and Roberts [22] and Chan et al. [31]:

$$K_C = \sigma_0 \sqrt{\pi a} F\left(\frac{a}{2\bar{y}}\right) \tag{4}$$

$$\sigma_0 = \frac{P_0 L_0 \bar{y}}{I} \tag{5}$$

where a is the pre-crack length and $\bar{y}$ is the vertical distance between the upper surface and the centroid of the cross-section. P_0 is the fracture load, L_0 is the longitudinal distance between the pre-crack and the indenter tip loading point and I is the second moment of area as derived by [22], for the pentagonal cross-section shape illustrated in Fig. 1.

$$I = \frac{wb^3}{12} + \left(y - \frac{b}{2}\right)^2 bw + \frac{w^4}{288} + \left[\frac{w}{6} + (b - y)\right]^2 \frac{w^2}{4} \tag{6}$$

$$y = \frac{\frac{b^2 w}{2} + \frac{w^2}{4}\left(b + \frac{w}{6}\right)}{bw + \frac{w^2}{4}} \tag{7}$$

The dimensionless shape factor $F\left(\frac{a}{2\bar{y}}\right)$ was determined using the equation derived by Chan et al. [31]:

$$F\left(\frac{a}{2\bar{y}}\right) = 3.71\left(\frac{a}{2\bar{y}}\right)^3 - 0.63\left(\frac{a}{2\bar{y}}\right)^2 + 0.242\frac{a}{2\bar{y}} + 0.974 \tag{8}$$

In the present microfracture experiments, typical values are $\frac{a}{2\bar{y}} = 0.23$ and F = 1.04.

Fracture tests were carried out on six cantilevers: three at the prior particle boundaries and three away from these boundaries. The toughness was found to be 1.5 ± 0.1 MPa·m$^{1/2}$ at the prior particle boundaries and 1.7 ± 0.1 MPa·m$^{1/2}$ far from them. This is lower than the value of 2.4 ± 0.3 MPa·m$^{1/2}$ reported earlier [13], which was obtained by measuring the length of cracks developed during microindentation.
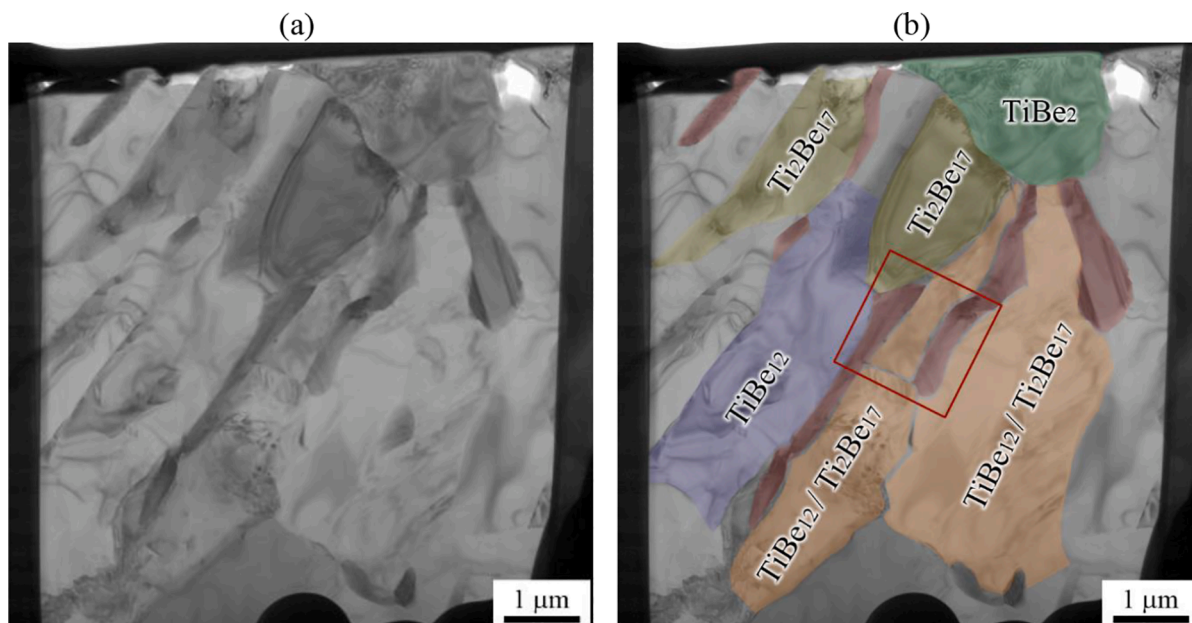
Fig. 7. (a) The overview of TEM lamella showing the cross-section microstructure of an undissolved particle in Be-Ti after extrusion and hot isostatic pressing at 1200 °C with (b) marked identified phases $TiBe_{12}$ (blue), Ti_2Be_{17} (yellow), $TiBe_2$ (green), as well as an undefined phase $TiBe_{12}$ or Ti_2Be_{17} (orange) and an unknown phase with a high content of titanium and impurity elements (red). The red square in (b) indicates the area of investigation in Fig. 8. (For interpretation of the references to colour in this figure legend, the reader is referred to the web version of this article.)
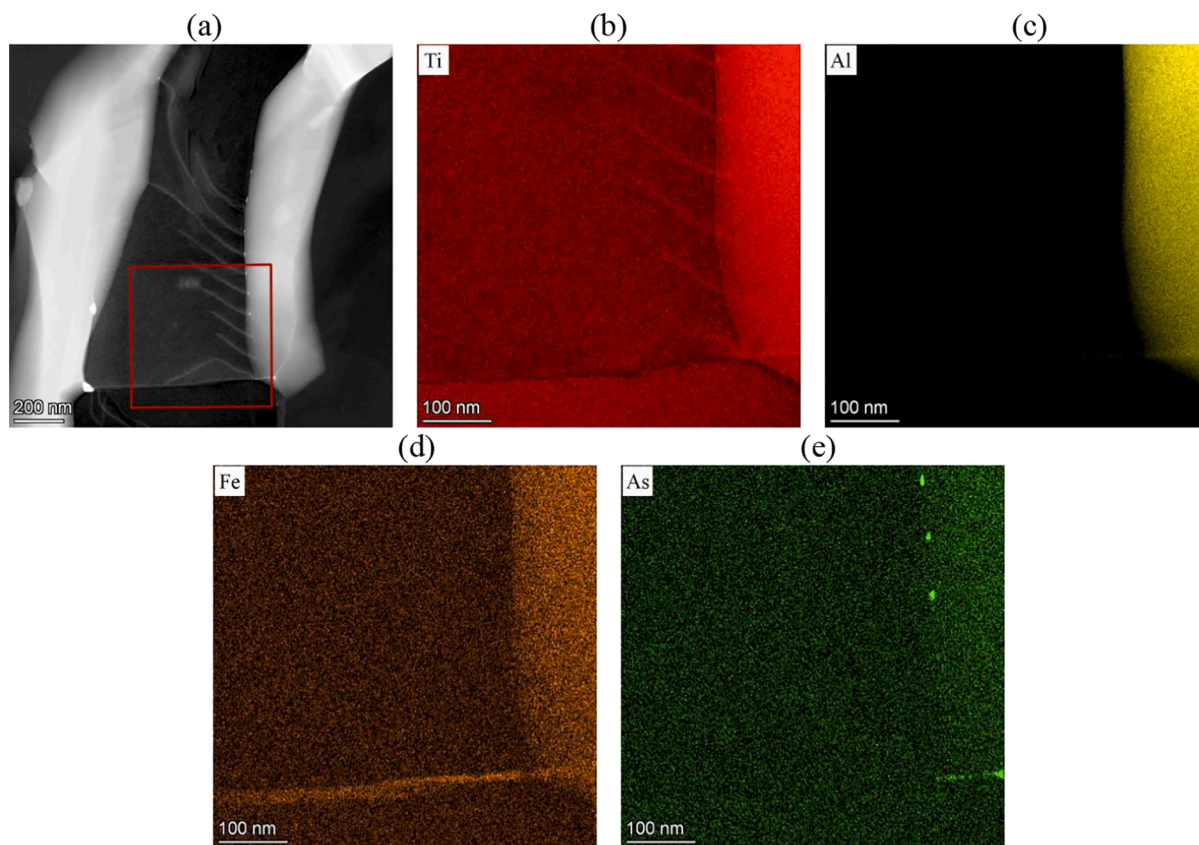
Fig. 8. (a) High-angle annular dark-field image of Be-Ti after extrusion and hot isostatic pressing at 1200 °C and EDS elemental maps corresponding to the area indicated by the red square in (a): (b) titanium, (c) aluminum, (d) iron, (e) arsenic. (For interpretation of the references to colour in this figure legend, the reader is referred to the web version of this article.)
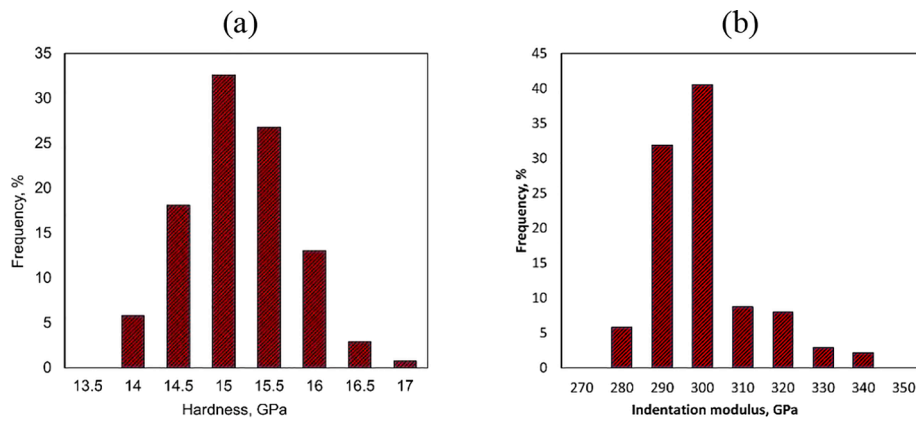
Fig. 9. The frequency distribution of the nanoindentation (a) hardness and (b) indentation modulus data obtained in Be-Ti after extrusion and HIP at 1100 °C. Average penetration depth is between 1300 and 1500 nm.
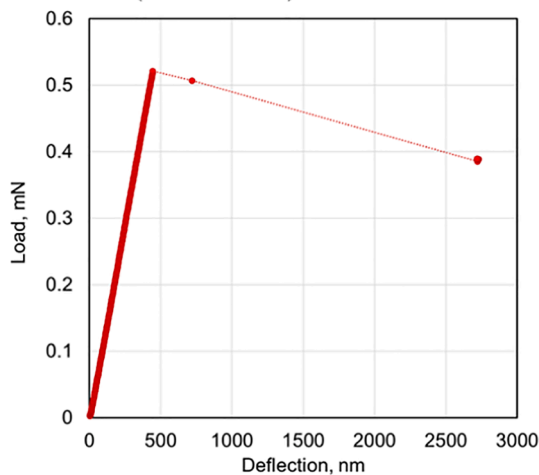

Fig. 10. Typical load–displacement curve of micro-scale pre-cracked cantilever from $TiBe_{12}$ samples tested at room temperature. No yield was observed before fracture occurred.

Some discrepancy can be explained both by the errors of both methods and by the volume of the material that was fractured during the bending of the microcantilevers and the microhardness indentation. The obtained toughness value is typical for hard brittle materials such as ceramics or intermetallics.

The critical stresses were 892 ± 47 MPa and 912 ± 86 MPa at the

prior particle boundaries and far from these boundaries, respectively. Both the average fracture toughness and the critical stress were slightly lower for the cantilevers prenothced for fracture at the prior particle boundaries, but the difference was close to or less than the uncertainty limit. This indicates that higher statistics are required to reliably compare local microstructural properties.

SEM analysis of the fractured cantilevers demonstrated that both type of cantilevers have very similar fracture surface topography. The materials fractured in a mixed mode of brittle inter- and transgranular fracture (Fig. 11). As demonstrated by a high-magnification image in Fig. 11b, some areas of the fracture surface show numerous facets with river pattern strips on the fracture surface typical for transgranular cleavage, another zones are featureless between ridges, indicating the intergranular surfaces. The microstructure of the fracture surface in Fig. 11b was used to determine the average grain size. It is about 0.4 μm, which is similar to the average grain size (0.64 μm) obtained by the EBSD measurement in Fig. 4b.

3.4. Mockup

Several additional capsules with extruded Be-Ti rods were prepared for the production of a mockup. The main goal was to demonstrate that it is possible to manufacture titanium beryllide blocks by hot extrusion and subsequent HIPing. In addition, the resulting mockup can be used for thermal cycling tests, since titanium beryllide will be rapidly heated up and cooled down during the cyclic operation of the fusion reactor. The capsules were subjected to HIP at 1100 or 1200 °C for 4 h.

Fig. 12a shows an open capsule after HIP at 1200 °C. In several places, the inner niobium layer interacted with the Be-Ti. Niobium was
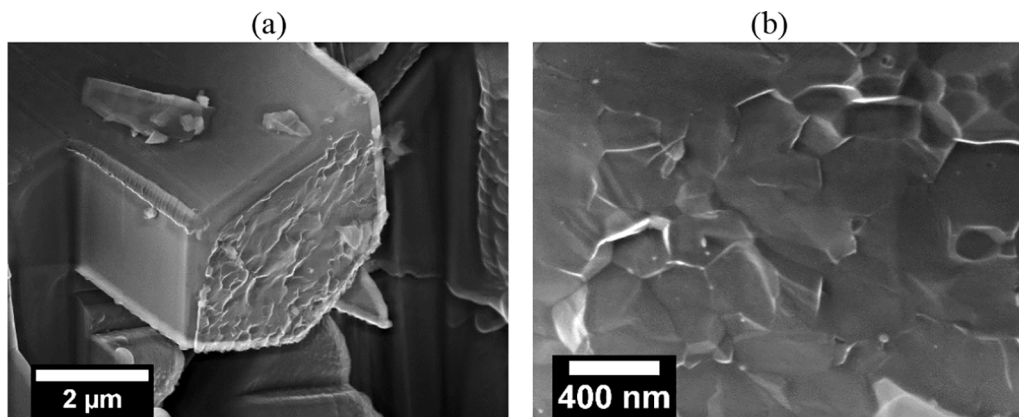

Fig. 11. (a) SEM image of the fractured cantilever in the $TiBe_{12}$ of Be-Ti sample after HIP at 1100 °C and (b) the corresponding fracture surface.
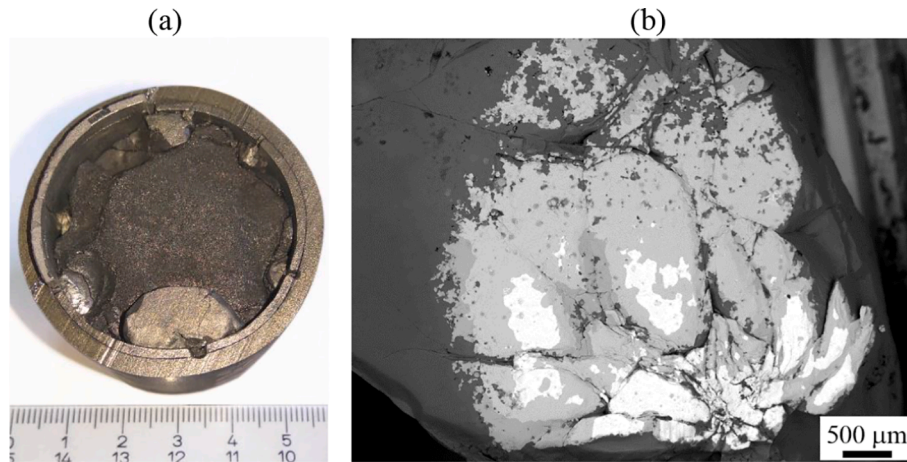
Fig. 12. Interaction of of the intermediate niobium layer with Be-Ti after HIP at 1200 °C: (a) after opening the capsule, (b) SEM BSE image of the region of such interaction with the formation of niobium beryllides.

previously selected as an interlayer material because it was found not to form any brittle diffusion layers at the interfaces "Be-Ti / Nb" and "Nb / CuCrZr" during extrusion [15,16]. However, at 1200 °C niobium can react with beryllium to form various niobium beryllides. Fig. 12b shows the zone of such interaction with distinct three Nb-containing phases in addition to the main TiBe$_{12}$ phase. This interaction leads not only to contamination with niobium but also cracking and fracture of titanium beryllide. Thus, the temperature of the HIP was limited by 1100° in order to avoid the interaction of Be-Ti with the niobium interlayer.

The opened capsule after the HIP at 1100 °C is shown in Fig. 13a. In this case, no interaction of Be-Ti with the niobium interlayer is observed, nevertheless, some chipping occurred in the edge of TiBe$_{12}$ during cutting. The diameter of the beryllide, taking into account the chipping zone, is about 25 mm. The resulting beryllide was used to cut a 4-fold reduced mockup of a breeder blanket block. The approximate outer diameter of the mockup is 20 mm, the height is 18 mm. As a result of electrical discharge machining, a mockup was manufactured without visible cracks and chips. The density of the mockup is measured as 2.255 g/cm^3 or 98.6% of the theoretical density. The results obtained have demonstrated the possibility of manufacturing complex products from titanium beryllide obtained by extrusion of Be-Ti powders and HIP. In the case of using rods four times larger in diameter than in the present work, full-size beryllide blocks can be manufactured.

4. Conclusions

The effect of HIP at 1000–1200 °C on the structure and properties of Be-Ti composites obtained by hot extrusion has been studied. The HIP resulted in an almost single-phase titanium beryllide (TiBe$_{12}$) with small amounts of Be and other phases. With an increase in the HIP temperature, the volume fraction of the beryllium phase and other intermediate beryllides decreases, and the density slightly increases from 98.4 to 99% of the theoretical density. EBSD maps showed that HIP at 1000 and 1100 °C provides a very fine-grained microstructure with an average grain size of 0.3 and 0.6 μm, respectively. HIP carried out at a higher temperature formed a coarser-grained structure of titanium beryllide with an average size of 3.4 μm. This treatment does not lead to complete dissolution of particles with an increased content of titanium and impurity elements. Even after HIP at 1200 °C, single particles with a complex structure are detected.
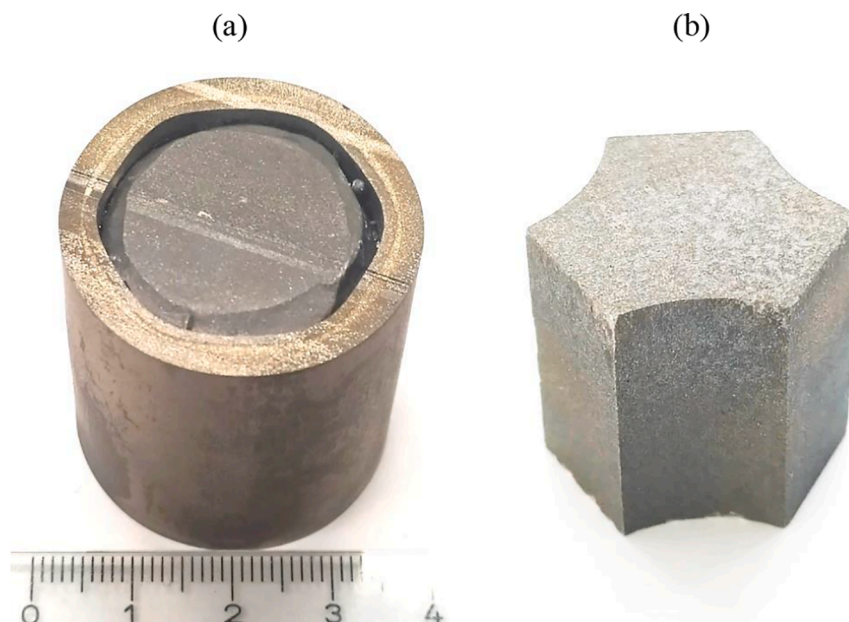

Fig. 13. (a) Opened Be-Ti capsule after extrusion and HIP at 1100 °C for 4 h and (b) a mockup cut out from it with dimensions of approximately Ø20 mm × 18 mm

The microhardness of Be-Ti composites gradually decreases from 1480 to 1350 $HV_{0.1}$ with an increase in the HIP temperature from 1000 to 1200 °C. Nanoindentation of the composite after HIP at 1100 °C showed a high hardness of $TiBe_{12}$ of 14.9 GPa, and also estimated its elastic modulus as 295 GPa. The fracture toughness of the same $TiBe_{12}$ was determined as 1.5–1.7 MPa·m$^{1/2}$ using results of fracture experiments of micromachined FIB cantilevers. According to the microstructural study of the fracture surface, the $TiBe_{12}$ cantilevers fractured in a mixed mode of brittle inter- and transgranular fracture.

On the basis of the results obtained in this work, the temperature of the HIP was chosen as 1100 °C, which was used for the final treatment of several additional capsules. The resulting titanium beryllide was successfully used to manufacture a reduced size mockup of Ø20 mm × 18 mm. The mockup has no visible surface defects and can be used for further experiments.

CRediT authorship contribution statement

Ramil Gaisin: Investigation, Writing – original draft, Writing – review & editing, Visualization, Methodology. **Viacheslav Kuksenko:** Methodology, Investigation, Visualization, Writing – original draft, Writing – review & editing. **Michael Duerrschnabel:** Methodology, Investigation, Writing – review & editing. **Vladimir Chakin:** Methodology, Supervision. **Aniceto Goraieb:** Methodology. **Pavel Vladimirov:** Supervision, Conceptualization, Funding acquisition, Writing – review & editing.

Declaration of Competing Interest

The authors declare that they have no known competing financial interests or personal relationships that could have appeared to influence the work reported in this paper.

Reference

[1] Francisco A. Hernández, Pavel Pereslavtsev, Guangming Zhou, Béla Kiss, Qinlan Kang, Heiko Neuberger, Vladimir Chakin, Ramil Gaisin, Pavel Vladimirov, Lorenzo V. Boccaccini, Gandolfo A. Spagnuolo, Salvatore D'Amico, Ivo Moscato, Advancements in the Helium-Cooled Pebble Bed Breeding Blanket for the EU DEMO: Holistic Design Approach and Lessons Learned, Fusion Sci. Technol. 75 (5) (2019) 352–364, https://doi.org/10.1080/15361055.2019.1607695.

[2] Pavel V. Vladimirov, Vladimir P. Chakin, Michael Dürrschnabel, Ramil Gaisin, Aniceto Goraieb, Francisco Alberto Hernandez Gonzalez, Michael Klimenkov, Michael Rieth, Rolf Rolli, Nikolai Zimber, Sergey Udartsev, Maxim Kolmakov, Anatoly Vechkutov, Evgeniy Frants, Development and characterization of advanced neutron multiplier materials, J. Nucl. Mater. 543 (2021) 152593, https://doi.org/10.1016/j.jnucmat.2020.152593.

[3] Ramil Gaisin, Vladimir Chakin, Pavel Vladimirov, Francisco A. Hernández, Sergey Udartsev, Anatoly Vechkutov, Maxim Kolmakov, Industrial-scale manufacturing experience of titanium beryllide block for DEMO blanket application, Fusion Eng. Des. 161 (2020) 111862, https://doi.org/10.1016/j.fusengdes.2020.111862.

[4] M. Nakamichi, J.-H. Kim, P. Kurinskiy, Characterization of vanadium beryllide pebble bed for the Japan DEMO blanket application, Fusion Eng. Des. 136 (2018) 125–127, https://doi.org/10.1016/j.fusengdes.2018.01.022.

[5] M. Nakamichi, J.H. Kim, P. Kurinskiy, M. Nakamura, Thermal properties of beryllides as advanced neutron multipliers for DEMO fusion application, Nuclear Materials and Energy 15 (2018) 71–75, https://doi.org/10.1016/j.nme.2018.02.002.

[6] M. Miyamoto, Y. Sugimoto, D. Nishijima, M.J. Baldwin, R.P. Doerner, A. Zaloznik, J.H. Kim, M. Nakamichi, Comparative study of surface modification and D retention between beryllium and beryllides under high flux plasma exposure, Nuclear Materials and Energy 27 (2021) 101014, https://doi.org/10.1016/j.nme.2021.101014.

[7] Vladimir Chakin, Rolf Rolli, Ramil Gaisin, Ursula Hoeppener-Kramar, Masaru Nakamichi, Milan Zmitko, Tritium release and retention in beryllium and titanium beryllide after neutron irradiation up to damage doses of 23–38 dpa, Fusion Eng. Des. 161 (2020) 111938, https://doi.org/10.1016/j.fusengdes.2020.111938.

[8] H. Kawamura, E. Ishitsuka, K. Tsuchiya, M. Nakamichi, M. Uchida, H. Yamada, K. Nakamura, H. Ito, T. Nakazawa, H. Takahashi, S. Tanaka, N. Yoshida, S. Kato, Y. Ito, Development of advanced blanket materials for a solid breeder blanket of a fusion reactor, Nucl. Fusion 43 (8) (2003) 675–680, https://doi.org/10.1088/0029-5515/43/8/306.

[9] J.-H. Kim, M. Nakamichi, Comparative study on arc-melted and plasma-sintered beryllides, J. Alloy. Compd. 546 (2013) 171–175, https://doi.org/10.1016/j.jallcom.2012.08.098.

[10] J. Shimwell, L. Lu, Y. Qiu, P. Pereslavtsev, A. Häußler, F. Hernández, C. Zeile, T. Eade, G.A. Spagnuolo, S. McIntosh, L. Packer, T. Barrett, Automated parametric neutronics analysis of the Helium Cooled Pebble Bed breeder blanket with Be12Ti, Fusion Eng. Des. 124 (2017) 940–943, https://doi.org/10.1016/j.fusengdes.2017.01.004.

[11] J.-H. Kim, M. Nakamichi, Optimization of synthesis conditions for plasma-sintered beryllium–titanium intermetallic compounds, J. Alloy. Compd. 577 (2013) 90–96, https://doi.org/10.1016/j.jallcom.2013.04.185.

[12] J.-H. Kim, M. Miyamoto, Y. Hujii, M. Nakamichi, Reactivity and deuterium retention properties of titanium-beryllium intermetallic compounds, Intermetallics 82 (2017) 20–25, https://doi.org/10.1016/j.intermet.2016.11.005.

[13] Ramil Gaisin, Vladimir Chakin, Rolf Rolli, Jan Hoffmann, Harald Leiste, Thomas Bergfeldt, Ute Jäntsch, Michael Klimenkov, Julia Lorenz, Aniceto Goraieb, Pavel Vladimirov, Anton Möslang, Synthesis of Be12Ti compound via arc melting or hot isostatic pressing, J. Alloy. Compd. 818 (2020) 152919, https://doi.org/10.1016/j.jallcom.2019.152919.

[14] R. Gaisin, V. Chakin, M. Duerrschnabel, R. Rolli, T. Weingaertner, A. Goraieb, P. Vladimirov, Effect of HIP at 800 and 900 °C on microstructure and properties of extruded Be-Ti composites, Nuclear Materials and Energy 24 (2020), 100771, https://doi.org/10.1016/j.nme.2020.100771.

[15] P. Kurinskiy, H. Leiste, A.A. Goraieb, S. Mueller, Hot extrusion of Be–Ti powder, Fusion Eng. Des. 98–99 (2015) 1817–1820, https://doi.org/10.1016/j.fusengdes.2015.04.037.

[16] P. Kurinskiy, H. Leiste, A. Goraieb, R. Rolli, S. Mueller, J. Reimann, A. Moeslang, Production of Be-Ti and Be-Zr rods by extrusion and their characterization, Fusion Eng. Des. 136 (2018) 49–52, https://doi.org/10.1016/j.fusengdes.2017.12.022.

[17] G.V. Samsonov, I.M. Vinitskii (Eds.), Handbook of Refractory Compounds, Springer US, Boston, MA, 1980.

[18] W.C. Oliver, G.M. Pharr, An improved technique for determining hardness and elastic modulus using load and displacement sensing indentation experiments, J. Mater. Res. 7 (6) (1992) 1564–1583, https://doi.org/10.1557/JMR.1992.1564.

[19] ISO 14577-1:2015. Metallic Materials – Instrumented Indentation Test for Hardness and Materials Parameters – Part 1: Test Method. 2015. 2nd ed. Geneva, Switzerland: ISO Central Secretariat.

[20] Xiankun Liu, Qijie Feng, Bin Tang, Jian Zheng, Zhou Zheng, Wei Zhou, Jiting Tian, Jing Wang, First-principles calculations of mechanical and thermodynamic properties of tetragonal Be12Ti, RSC Adv. 9 (10) (2019) 5302–5312, https://doi.org/10.1039/C8RA08711C.

[21] A.C. Fischer-Cripps, Nanoindentation. Mechanical Engineering Series., New York, NY: Springer New York., 2004.

[22] D. Di Maio, S.G. Roberts, Measuring fracture toughness of coatings using focused-ion-beam-machined microbeams, J. Mater. Res. 20 (2) (2005) 299–302, https://doi.org/10.1557/JMR.2005.0048.

[23] L.A Charlot, J.L Brimhall, L.E Thomas, S.M Bruemmer, J.P Hirth, Twinning relationship in Be12Nb, Scr. Metall. Mater. 25 (1) (1991) 99–103, https://doi.org/10.1016/0956-716X(91)90361-4.

[24] S.M. Bruemmer, L.A. Charlot, J.L. Brimhall, C.H. Henager, J.P. Hirth, Dislocation structures in be12nb after high-temperature deformation, Philos. Mag. A 65 (5) (1992) 1083–1094, https://doi.org/10.1080/01418619208201497.

[25] V. Chakin, R. Rolli, A. Moeslang, P. Kurinskiy, P. Vladimirov, C. Dorn, I. Kupriyanov, Tritium release from advanced beryllium materials after loading by tritium/hydrogen gas mixture, Fusion Eng. Des. 107 (2016) 75–81, https://doi.org/10.1016/j.fusengdes.2016.04.018.

[26] D.V. Bachurin, P.V. Vladimirov, Ab initio study of Be and Be12Ti for fusion applications, Intermetallics 100 (2018) 163–170, https://doi.org/10.1016/j.intermet.2018.06.009.

[27] R.L. Fleischer, R.J. Zabala, Mechanical Properties of High-Temperature Beryllium Intermetallic Compounds, Metall. Trans. A 20 (7) (1989) 1279–1282.

[28] R.L. Fleischer, R.J. Zabala, Mechanical properties of high-temperature titanium intermetallic compounds, Metall. Trans. A 21 (7) (1990) 1951–1957, https://doi.org/10.1007/BF02647243.

[29] R. M. Paine, A. Stonehouse, W. W. Beaver, DEVELOPMENT OF INTERMETALLIC COMPOUNDS FOR VERY HIGH TEMPERATURE APPLICATIONS. Quarterly Progress Report, January 1, 1962 through March 31, 1962, in: 1962.

[30] T.G. Nieh, J. Wadsworth, F.C. Grensing, J.-M. Yang, Mechanical properties of vanadium beryllide, VBe12, J. Mater. Sci. 27 (10) (1992) 2660–2664, https://doi.org/10.1007/BF00540686.

[31] H. Chan, S.G. Roberts, J. Gong, Micro-scale fracture experiments on zirconium hydrides and phase boundaries, J. Nucl. Mater. 475 (2016) 105–112, https://doi.org/10.1016/j.jnucmat.2016.03.026.